Effect of spatial coherence on propagation, tight focusing, and radiation forces of an azimuthally polarized beam

Yiming Dong,[1,2] Fei Wang,[1] Chengliang Zhao,[1] and Yangjian Cai[1,*]
[1]*School of Physical Science and Technology, Soochow University, Suzhou 215006, China*
[2]*Department of Physics, Shaoxing University, Shaoxing 312000, China*
(Received 13 June 2012; published 26 July 2012)

We report experimental generation of an azimuthally polarized (AP) beam with variable spatial coherence. The effect of spatial coherence on the propagation properties of an AP beam is studied both numerically and experimentally, and our experimental results agree well with the theoretical predictions. The dependence of the intensity distribution of an AP beam focused by a high numerical aperture objective lens on its initial spatial coherence is illustrated numerically, and it is found that we can shape the beam profile of a tightly focused AP beam by varying its initial spatial coherence. Furthermore, the radiation forces on Rayleigh particles induced by a tightly focused AP beam are studied, and we find that the tightly focused AP beam can be used to trap a Rayleigh particle whose refractive index is larger or smaller than that of the ambient by varying its initial spatial coherence. Our results will be useful for particle trapping and material thermal processing.

DOI: 10.1103/PhysRevA.86.013840 PACS number(s): 42.25.Ja, 42.25.Kb, 41.85.Ew, 87.80.Cc

I. INTRODUCTION

In past years, cylindrical vector beams, such as radially and azimuthal polarized beams, have been explored extensively due to their wide applications in microscopy, lithography, free-space optical communications, electron acceleration, particle trapping, material processing, optical data storage, high-resolution metrology, superresolution imaging, plasmonic focusing, and laser machining. [1–31] Different methods have been developed to generate various cylindrical vector beams. [1,16–20] The unique focusing properties of cylindrical vector beams by a high numerical aperture (NA) objective lens have been investigated widely. [1,4,8,21–31] When a radially polarized (RP) beam is focused by a high NA objective lens, a strong longitudinal electric field appears and the tightly focused beam spot of a RP beam is much smaller than that of a linearly polarized beam, [1,4] and the focused beam spot can be used to trap a Rayleigh particle whose refractive index is larger than that of the ambient. [11,12] When an azimuthally polarized (AP) beam is focused by a high NA objective lens, a strong magnetic field on the optical axis is generated while the electric field is purely transverse and the focused beam spot has a dark hollow beam profile, [1,4] which can be used to trap a Rayleigh particle whose refractive index is smaller than that of the ambient. [13] The polarization rotator setup was proposed by Zhan and Leger in [24] to generate a generalized cylindrical vector beam which can be decomposed into a linear superposition of RP and AP components, and it is found that we can shape the tightly focused beam profile of a generalized cylindrical vector beam by adjusting the rotating angle of the polarization rotator, which can be used to trap a Rayleigh particle whose refractive index is larger or smaller than that of the ambient. Zhang *et al*. studied the focusing properties of a double-ring-shaped RP beam, and found that the tightly focused beam spot of a double-ring-shaped RP beam also can be used to trap different particles by changing the truncation parameter. [14]

More recently, Dong *et al*. extended the cylindrical vector beam to the partially coherent case with the help of the unified theory of coherence and polarization, [32] and studied its paraxial propagation properties in free space theoretically. It was shown that the propagation properties of a cylindrical vector beam are significantly affected by its initial spatial coherence. More recently, Wang *et al*. reported experimental generation of a partially coherent RP beam. [33] In the present article, we first report experimental generation of an AP beam with variable spatial coherence, and verify the effect of spatial coherence on the propagation properties of an AP beam. The influence of spatial coherence on the intensity distribution of an AP beam focused by a high NA objective lens and its radiation forces on Rayleigh particles is illustrated numerically. We show that a tightly focused AP beam can be used to trap different particles by varying its initial spatial coherence.

II. PARTIALLY COHERENT AP BEAM AND ITS PARAXIAL PROPAGATION FORMULA

In this section, we outline briefly the theoretical model for a partially coherent AP beam and its paraxial propagation formula. The vectorial electric field of a coherent AP beam is expressed as the superposition of orthogonally polarized Hermite Gaussian HG_{01} and HG_{10} modes [1]

$$\begin{aligned}\vec{\mathbf{E}}(x,y) &= E_x(x,y)\,\vec{\mathbf{e}}_x + E_y(x,y)\,\vec{\mathbf{e}}_y \\ &= E_0\left[-\frac{y}{w_0}\exp\left(-\frac{x^2+y^2}{w_0^2}\right)\vec{\mathbf{e}}_x\right. \\ &\quad \left. + \frac{x}{w_0}\exp\left(-\frac{x^2+y^2}{w_0^2}\right)\vec{\mathbf{e}}_y\right], \end{aligned} \tag{1}$$

where w_0 denotes the beam waist size of a fundamental Gaussian mode and E_0 is a normalization factor. The power of the AP beam is calculated by the following formula:

$$\eta_{\text{power}} = \int_{-\infty}^{+\infty}\int_{-\infty}^{+\infty}\frac{\varepsilon_0 c}{2}[|E_x(x,y)|^2 + |E_y(x,y)|^2]dx\,dy, \tag{2}$$

where ε_0 and c represent the dielectric constant and the light speed in vacuum, respectively. Applying Eqs. (1) and (2), we

*yangjiancai_1977@yahoo.com.cn

find that E_0 is related to η_{power} as follows:

$$E_0 = \sqrt{\frac{8\eta_{\text{power}}}{\pi\varepsilon_0 c w_0^2}}. \tag{3}$$

Based on the unified theory of coherence and polarization, the second-order correlation properties of a paraxial partially coherent vector beam at $z = 0$, in space-frequency domain, can be characterized by the 2×2 cross-spectral density (CSD) matrix of the electric field, defined by the formula [34,35]

$$\hat{W}^{(ee)}(x_1,y_1,x_2,y_2,0) = \begin{pmatrix} W_{xx}^{(ee)}(x_1,y_1,x_2,y_2,0) & W_{xy}^{(ee)}(x_1,y_1,x_2,y_2,0) \\ W_{yx}^{(ee)}(x_1,y_1,x_2,y_2,0) & W_{yy}^{(ee)}(x_1,y_1,x_2,y_2,0) \end{pmatrix}, \tag{4}$$

with elements

$$W_{\alpha\beta}^{(ee)}(x_1,y_1,x_2,y_2,0) = \langle E_\alpha(x_1,y_1,0)E_\beta^*(x_2,y_2,0)\rangle \quad (\alpha = x,y;\beta = x,y), \tag{5}$$

where (x_1,y_1) and (x_2,y_2) denote the coordinates of two arbitrary points at the source plane, and E_x and E_y denote the components of the random electric vector, along two mutually orthogonal x and y directions perpendicular to the z axis. Here the asterisk denotes the complex conjugate and the angular brackets denote ensemble average.

We assume that a partially coherent AP beam is radiated from a Schell-model source, [35,36] then the element of its CSD matrix can be expressed as follows: [32]

$$W_{xx}^{(ee)}(x_1,y_1,x_2,y_2,0) = E_0^2\frac{y_1y_2}{w_0^2}\exp\left[-\frac{x_1^2+y_1^2+x_2^2+y_2^2}{w_0^2} - \frac{(x_1-x_2)^2+(y_1-y_2)^2}{2\sigma_{xx}^2}\right], \tag{6}$$

$$W_{xy}^{(ee)}(x_1,y_1,x_2,y_2,0) = -E_0^2B_{xy}\frac{y_1x_2}{w_0^2}\exp\left[-\frac{x_1^2+y_1^2+x_2^2+y_2^2}{w_0^2} - \frac{(x_1-x_2)^2+(y_1-y_2)^2}{2\sigma_{xy}^2}\right], \tag{7}$$

$$W_{yx}^{(ee)}(x_1,y_1,x_2,y_2,0) = W_{xy}^{(ee)*}(x_1,y_1,x_2,y_2,0), \tag{8}$$

$$W_{yy}^{(ee)}(x_1,y_1,x_2,y_2,0) = E_0^2\frac{x_1x_2}{w_0^2}\exp\left[-\frac{x_1^2+y_1^2+x_2^2+y_2^2}{w_0^2} - \frac{(x_1-x_2)^2+(y_1-y_2)^2}{2\sigma_{yy}^2}\right], \tag{9}$$

where $B_{xy} = |B_{xy}|\exp(i\phi)$ is the correlation coefficient between the E_x and E_y field components, ϕ is the phase difference between the x and y components of the field and is removable in most cases, and σ_{xx}, σ_{yy}, and σ_{xy} are the widths of autocorrelation functions of the x component of the field, of the y component of the field, and of the mutual correlation function of x and y field components, respectively.

After passing through a paraxial *ABCD* optical system, the elements of the CSD matrix of a partially coherent AP beam are written as [32]

$$\begin{aligned} W_{xx}^{(ee)}(u_1,v_1,u_2,v_2,z) = {} & \frac{E_0^2\pi^2}{8\sigma_{xx}^2M_{1xx}^2M_{2xx}^3w_0^2}\left(\frac{1}{\lambda|B|}\right)^2\exp\left[\frac{ikD}{2B}\left(u_1^2+v_1^2\right) - \frac{ikD^*}{2B^*}\left(u_2^2+v_2^2\right)\right] \\ & \times\exp\left[-\frac{k^2\left(u_1^2+v_1^2\right)}{4M_{1xx}B^2} - \frac{4k^2M_{1xx}^2B^2\sigma_{xx}^4\left(u_2^2+v_2^2\right)+k^2(B^*)^2\left(u_1^2+v_1^2\right)-4k^2M_{1xx}|B|^2\sigma_{xx}^2(u_1u_2+v_1v_2)}{16M_{1xx}^2M_{2xx}|B|^4\sigma_{xx}^4}\right] \\ & \times\left[-k^2\left(\frac{2M_{1xx}B\sigma_{xx}^2v_2 - B^*v_1}{2M_{1xx}|B|^2\sigma_{xx}^2}\right)^2 + \frac{2M_{2xx}k^2\sigma_{xx}^2v_1}{B}\left(\frac{2M_{1xx}B\sigma_{xx}^2v_2 - B^*v_1}{2M_{1xx}|B|^2\sigma_{xx}^2}\right) + 2M_{2xx}\right], \end{aligned} \tag{10}$$

$$\begin{aligned} W_{xy}^{(ee)}(u_1,v_1,u_2,v_2,z) = {} & \frac{B_{xy}E_0^2k^2\pi^2}{8M_{1xy}^2M_{2xy}^3\sigma_{xy}^2w_0^2}\left(\frac{1}{\lambda|B|}\right)^2\exp\left[\frac{ikD}{2B}\left(u_1^2+v_1^2\right) - \frac{ikD^*}{2B^*}\left(u_2^2+v_2^2\right)\right] \\ & \times\exp\left[-\frac{k^2\left(u_1^2+v_1^2\right)}{4M_{1xy}B^2} - \frac{4k^2M_{1xy}^2B^2\sigma_{xy}^4\left(u_2^2+v_2^2\right)+k^2(B^*)^2\left(u_1^2+v_1^2\right)-4k^2M_{1xy}|B|^2\sigma_{xy}^2(u_1u_2+v_1v_2)}{16M_{1xy}^2M_{2xy}|B|^4\sigma_{xy}^4}\right] \\ & \times\left(\frac{u_2}{B^*} - \frac{u_1}{2M_{1xy}B\sigma_{xy}^2}\right)\left(\frac{v_2}{B^*} - \frac{1+4M_{1xy}M_{2xy}\sigma_{xy}^4}{2M_{1xy}B\sigma_{xy}^2}v_1\right), \end{aligned} \tag{11}$$

$$W_{yx}^{(ee)}(u_1,v_1,u_2,v_2,z) = W_{xy}^{(ee)*}(u_2,v_2,u_1,v_1,z), \tag{12}$$

$$W_{yy}^{(ee)}(u_1,v_1,u_2,v_2,z) = \frac{E_0^2\pi^2}{8\sigma_{yy}^2 M_{1yy}^2 M_{2yy}^3 w_0^2}\left(\frac{1}{\lambda|B|}\right)^2 \exp\left[\frac{ikD}{2B}\left(u_1^2+v_1^2\right)-\frac{ikD^*}{2B^*}\left(u_2^2+v_2^2\right)\right]$$
$$\times \exp\left[-\frac{k^2\left(u_1^2+v_1^2\right)}{4M_{1yy}B^2}-\frac{4k^2M_{1yy}^2B^2\sigma_{yy}^4\left(u_2^2+v_2^2\right)+k^2(B^*)^2\left(u_1^2+v_1^2\right)-4k^2M_{1yy}|B|^2\sigma_{yy}^2(u_1u_2+v_1v_2)}{16M_{1yy}^2M_{2yy}|B|^4\sigma_{yy}^4}\right]$$
$$\times\left[-k^2\left(\frac{2M_{1yy}B\sigma_{yy}^2u_2-B^*u_1}{2M_{1yy}|B|^2\sigma_{yy}^2}\right)^2+\frac{2M_{2yy}k^2\sigma_{yy}^2u_1}{B}\left(\frac{2M_{1yy}B\sigma_{yy}^2u_2-B^*u_1}{2M_{1yy}|B|^2\sigma_{yy}^2}\right)+2M_{2yy}\right], \quad (13)$$

with

$$M_{1xx} = 1/w_0^2+1/\left(2\sigma_{xx}^2\right)-ikA/(2B), \qquad M_{2xx} = 1/w_0^2+1/\left(2\sigma_{xx}^2\right)+ikA^*/\left(2B^*\right)-1/\left(4M_{1xx}\sigma_{xx}^4\right),$$
$$M_{1xy} = 1/w_0^2+1/\left(2\sigma_{xy}^2\right)-ikA/(2B), \qquad M_{2xy} = 1/w_0^2+1/\left(2\sigma_{xy}^2\right)+ikA^*/\left(2B^*\right)-1/\left(4M_{1xy}\sigma_{xy}^4\right), \quad (14)$$
$$M_{1yy} = 1/w_0^2+1/\left(2\sigma_{yy}^2\right)-ikA/(2B), \qquad M_{2yy} = 1/w_0^2+1/\left(2\sigma_{yy}^2\right)+ikA^*/\left(2B^*\right)-1/\left(4M_{1yy}\sigma_{yy}^4\right).$$

Here A, B, C, and D are the transfer matrix elements of the optical system, (u_1,v_1) and (u_2,v_2) denote the coordinates of two arbitrary points at the output plane, and $k = 2\pi/\lambda$ is the wave number with λ being the wavelength.
The intensity of the partially coherent AP beam at the output plane is expressed as

$$I(u,v,z) = \mathrm{Tr}[\hat{W}^{(ee)}(u,v,u,v,z)] = W_{xx}^{(ee)}(u,v,u,v,z)+W_{yy}^{(ee)}(u,v,u,v,z). \quad (15)$$

Applying Eqs. (11)–(15), we can study the propagation properties of a partially coherent AP beam through a paraxial *ABCD* optical system in free space conveniently.

III. EXPERIMENTAL GENERATION OF A PARTIALLY COHERENT AP BEAM

In this section, we report experimental generation of an AP beam with variable spatial coherence, and verify the effect of spatial coherence on the propagation properties of an AP beam.

Part 1 of Fig. 1 shows our experimental setup for generating an AP beam with variable spatial coherence. A linearly polarized beam generated by a He-Ne laser is focused by a thin lens L_1, then it illuminates a rotating ground-glass disk (RGGD), producing a partially coherent beam with Gaussian statistics. After passing through a collimation lens L_2 and a Gaussian amplitude filter (GAF), the generated partially coherent beam becomes a linearly polarized Gaussian Schell-model (GSM) beam, whose intensity distribution and spectral degree of coherence satisfy Gaussian distribution. After passing through a liquid crystal polarization converter (Acroptix, Switzerland), the generated GSM beam becomes a partially coherent AP beam.

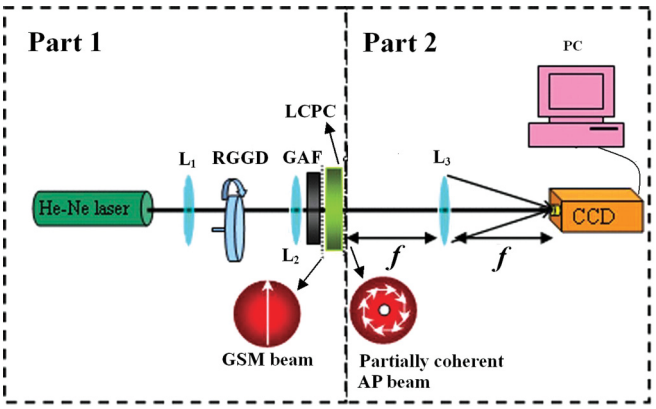

FIG. 1. (Color online) Experimental setup for generating a partially coherent AP beam and measuring its intensity distribution after passing through a thin lens. L_1, L_2, and L_3, thin lenses; RGGD, rotating ground-glass disk; GAF, Gaussian amplitude filter; LCPC, liquid crystal polarization converter; CCD, charge-coupled device; PC, personal computer.

The second-order correlation properties of a linearly polarized GSM beam at $z = 0$ is characterized by the CSD given by [36,37]

$$W_{\mathrm{GSM}}^{(ee)}(x_1,y_1,x_2,y_2,0) = \exp\left[-\frac{x_1^2+y_1^2+x_2^2+y_2^2}{w_0^2}-\frac{(x_1-x_2)^2+(y_1-y_2)^2}{2\sigma_0^2}\right], \quad (16)$$

where w_0 and σ_0 represent the beam waist size and the transverse coherence width, respectively. The transmission function of the GAF determines the value of w_0, and w_0 is

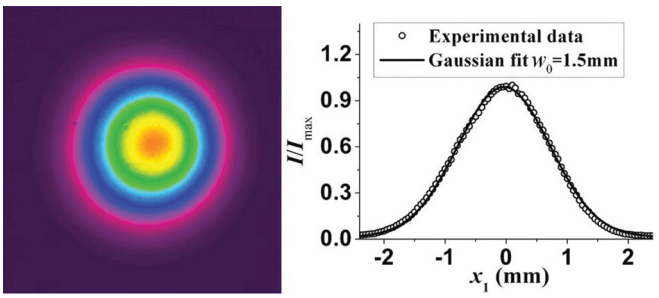

FIG. 2. (Color online) Experimental results of the intensity distribution of the generated GSM beam just behind the GAF and the corresponding cross line (dotted curve). The solid curve is a result of the Gaussian fit.

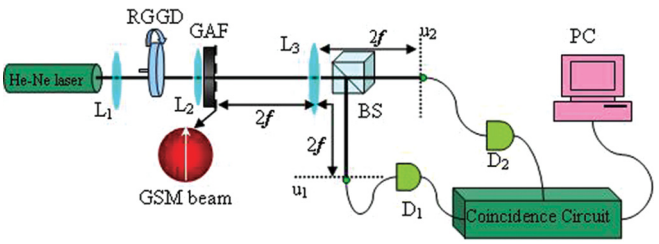

FIG. 3. (Color online) Experimental setup for measuring the transverse coherence width σ_0 of the generated GSM beam. BS, 50:50 beam splitter; D_1 and D_2, single photon detectors; PC, personal computer.

equal to 1.5 mm in our experiment (see Fig. 2). The transverse coherence width σ_0 is determined by the focused beam spot size on the RGGD and the roughness of the RGGD together. In our experiment, the roughness of the RGGD is fixed and we mainly modulate the value of σ_0 by varying the focused beam spot on the RGGD (i.e., the distance between L_1 and RGGD).

We adopt the method proposed in [37] to measure the transverse coherence width σ_0 of the generated GSM beam. Figure 3 shows our experimental setup for measuring σ_0. After passing through a thin lens L_3, the generated GSM beam is split into two beams by a beam splitter. The reflected and transmitted beams arrive at D_1 and D_2, which scan the transverse planes of u_1 and u_2, respectively. Both the distances from the GAF to L_3 and from L_3 to D_1 and D_2 are $2f$ (i.e., $2f$-imaging system). The electronic coincidence circuit is used to measure the fourth-order correlation function (i.e., intensity correlation function) between two detectors. The normalized fourth-order correlation between two detectors is expressed as

$$g^{(2)}(u_1-u_2,\tau)=\frac{\langle I(u_1,t)I(u_2,t+\tau)\rangle}{\langle I(u_1,t)\rangle\,\langle I(u_2,t+\tau)\rangle}, \tag{17}$$

where $\langle I(u_1,t)\rangle$ and $\langle I(u_2,t+\tau)\rangle$ are the average intensities at two detectors, respectively, and τ denotes the delay time of the photon flux of two optical paths. Applying the Gaussian moment theorem, [36] $g^{(2)}(u_1-u_2,\tau)$ of the generated GSM beam with $\tau=0$ is simplified as

$$g^{(2)}(u_1-u_2,\tau=0)=1+\exp\left[-(u_1-u_2)^2/2\sigma_0^2\right]. \tag{18}$$

To measure σ_0, D_2 is fixed at $u_2=0$ and D_1 scans along the plane u_1. Then we can obtain the distribution of the normalized fourth-order correlation function with $\tau=0$ between two detectors from the electronic coincidence circuit.

Figure 4 shows our experimental results (dotted curves) of the normalized fourth-order correlation function for three different focused beam spot sizes on the RGGD. From the Gaussian fits (solid curves) of the experimental results, we obtain $\sigma_0=1.5$ mm, $\sigma_0=0.7$ mm, and $\sigma_0=0.3$ mm for Figs. 4(a)–4(c), respectively. If there is no RGGD in Fig. 3, σ_0 is approximated as $\sigma_0=\infty$. In our experiment, the liquid crystal polarization located just behind the GAF is used to convert the generated GSM beam into a partially coherent AP beam; it just modulates the state of polarization of the GSM beam, while it does not alter its spatial coherence, thus the correlation coefficients of the generated partially coherent AP beam are approximated as $\sigma_{xx}=\sigma_{yy}=\sigma_{xy}=\sigma_0$.

Part II of Fig. 1 shows the setup for measuring the intensity of a partially coherent AP beam at the focal plane after passing through a thin lens L_3 with focal length $f=40$ cm. The distance from the liquid crystal polarization converter to L_3 and the distance from L_3 to CCD are both equal to f. The transfer matrix between the liquid crystal polarization converter and CCD reads as

$$\begin{pmatrix} A & B \\ C & D \end{pmatrix}=\begin{pmatrix} 1 & f \\ 0 & 1 \end{pmatrix}\begin{pmatrix} 1 & 0 \\ -1/f & 1 \end{pmatrix}\begin{pmatrix} 1 & f \\ 0 & 1 \end{pmatrix}=\begin{pmatrix} 0 & f \\ -1/f & 0 \end{pmatrix}. \tag{19}$$

With the measured beam parameters, Eq. (19) and the obtained propagation formulas in Sec. II, we can simulate the focusing properties of a partially coherent AP beam, and carry out comparison with experimental results.

Figure 5 shows our experimental results of the intensity distribution of the focused AP beam with variable initial spatial coherence and the corresponding cross line at the focal plane. For the convenience of comparison, the corresponding results calculated by the theoretical formulas are also shown in Fig. 5. As shown in Fig. 5, the focused beam spot of a coherent AP beam with $\sigma_0=\infty$ still has a dark hollow beam profile as expected. With the decrease of σ_0 (i.e., decrease of spatial coherence), the focused beams spot gradually transforms from a dark hollow beam profile into a Gaussian beam profile [see Figs. 5(a)–5(d)]. For a suitable value of σ_0, a focused beam spot with a flat-topped beam profile can be formed [see Fig. 5(b)]. Our experimental results agree reasonably well with the theoretical predictions. Thus, decreasing the spatial coherence of an AP beam provides a convenient way for shaping its beam profile on propagation.

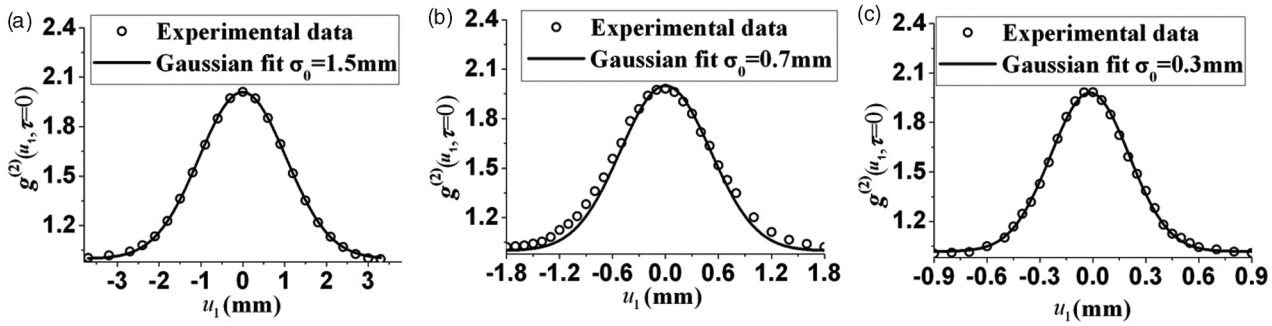

FIG. 4. Experimental results of the normalized fourth-order correlation function (dotted curve) and the corresponding Gaussian fit (solid curve) for three different focused beam spot sizes on the RGGD.

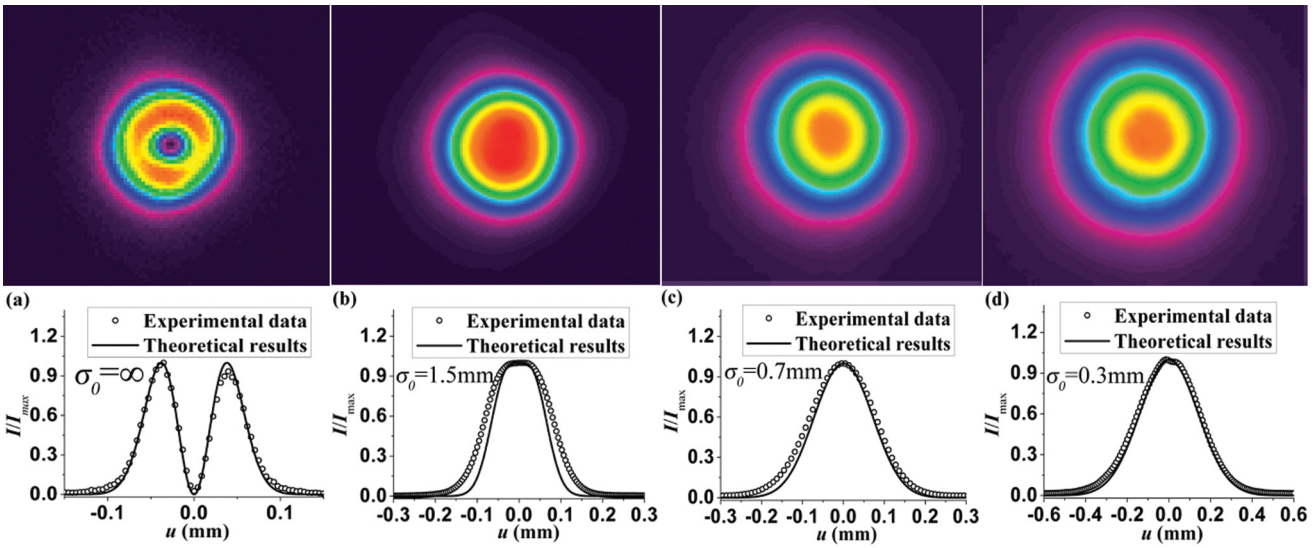

FIG. 5. (Color online) Experimental results of the intensity distribution of the focused AP beam and the corresponding cross line (dotted curve) at the focal plane for different values of σ_0. The solid curves are calculated by the theoretical formulas.

To learn about the effect of spatial coherence on the propagation properties of the orthogonally polarized Hermite Gaussian HG_{01} and HG_{10} modes which consist of the AP beam, we now carry out experimental study of the focusing properties of a partially coherent AP beam after passing through a linear polarizer. A linear polarizer whose transmission axis forms an angle φ with the x axis is located just behind the liquid crystal polarization converter. The intensity distribution of the partially coherent AP beam in the focal plane can be written as

$$I_\varphi(x,y,z) = W_{xx}^{(ee)}(x,y,x,y,z)\cos^2\varphi + W_{yy}^{(ee)}(x,y,x,y,z) \times \sin^2\varphi + W_{xy}^{(ee)}(x,y,x,y,z)\sin 2\varphi. \quad (20)$$

Figure 6 shows our experimental results of the focused beam profile of an AP beam with variable spatial coherence after passing through a linear polarizer for different transmission angle φ. One finds from Fig. 6 that the orthogonally polarized Hermite Gaussian HG_{01} ($\varphi = 0$) and HG_{10} ($\varphi = 90^o$) modes are strongly influenced by the initial spatial coherence. With the decrease of initial spatial coherence, both the focused beam spots of HG_{01} and HG_{10} gradually degenerate into circular Gaussian beam profiles.

IV. INTENSITY DISTRIBUTION OF A PARTIALLY COHERENT AP BEAM FOCUSED BY A HIGH NA OBJECTIVE LENS

In many practical applications, the cylindrical vector beam usually is focused by a high NA objective lens and the focused beam spot size is comparable to the wavelength of the beam. In this case, the paraxial propagation theory is no longer valid to study the focusing properties of the cylindrical vector beam. In this section, we adopt the Richards-Wolf vectorial diffraction integral to study the effect of spatial coherence on the intensity distribution of an AP beam focused by a high NA objective lens numerically. Figure 7 shows the scheme of a tightly focusing system.

According to the Richards-Wolf diffraction integral, in the cylindrical coordinate system, the vectorial electric field of a tightly focused cylindrical vector beam at the focal plane is expressed as [1,4,8,21–31]

$$\vec{\mathbf{E}}(r,\varphi,z) = -\frac{\mathrm{if}\sqrt{n_1}}{\lambda}\int_0^{\theta_{\max}}\int_0^{2\pi}\sqrt{\cos\theta}\,\sin\theta\,\exp\{ik_1[z\cos\theta + r\sin\theta\cos(\phi-\varphi)]\} \times \begin{bmatrix} l_x(\theta,\phi)[\cos\theta + \sin^2\phi(1-\cos\theta)] + l_y(\theta,\phi)\cos\phi\,\sin\phi(\cos\theta-1) \\ l_x(\theta,\phi)\cos\phi\,\sin\phi(\cos\theta-1) + l_y(\theta,\phi)[\cos\theta + \cos^2\phi(1-\cos\theta)] \\ -l_x(\theta,\phi)\cos\phi\,\sin\theta - l_y(\theta,\phi)\sin\phi\,\sin\theta \end{bmatrix} d\theta\,d\phi, \quad (21)$$

where r, φ, and z are the cylindrical coordinates of an observation point, φ is the azimuthal angle of the incident beam, f is the focal length of the lens, $k_1 = kn_1 = 2\pi n_1/\lambda$ is the wave number in the surrounding medium with n_1 being the refractive index of the surrounding medium, θ is the NA angle, and $\theta_{\max}$ is the maximal NA angle which is related to the NA by the formula $\theta_{\max} = \arcsin \mathrm{NA}/n_1$, $l_x(\theta,\phi)$, and $l_y(\theta,\phi)$ are the pupil apodization functions at the aperture surface and are derived by setting $r = f\,\sin\theta$ in $E_x(x,y)$ and $E_y(x,y)$, respectively.

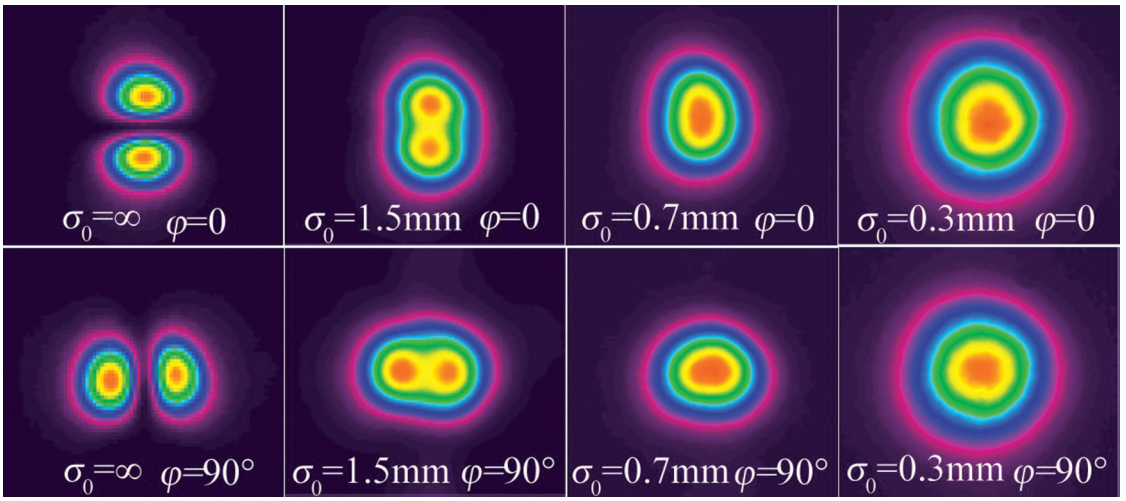

FIG. 6. (Color online) Experimental results of the focused beam profile of an AP beam with variable spatial coherence after passing through a linear polarizer for different transmission angle φ.

Applying Eq. (21), the 3 × 3 CSD matrix of the electric field in the focal region is expressed as

$$\hat{W}^{(ee)}(r_1,\varphi_1,z_1,r_2,\varphi_2,z_2)=\begin{pmatrix} W_{xx}^{(ee)}(r_1,\varphi_1,z_1,r_2,\varphi_2,z_2) & W_{xy}^{(ee)}(r_1,\varphi_1,z_1,r_2,\varphi_2,z_2) & W_{xz}^{(ee)}(r_1,\varphi_1,z_1,r_2,\varphi_2,z_2)\\ W_{yx}^{(ee)}(r_1,\varphi_1,z_1,r_2,\varphi_2,z_2) & W_{yy}^{(ee)}(r_1,\varphi_1,z_1,r_2,\varphi_2,z_2) & W_{yz}^{(ee)}(r_1,\varphi_1,z_1,r_2,\varphi_2,z_2)\\ W_{zx}^{(ee)}(r_1,\varphi_1,z_1,r_2,\varphi_2,z_2) & W_{zy}^{(ee)}(r_1,\varphi_1,z_1,r_2,\varphi_2,z_2) & W_{zz}^{(ee)}(r_1,\varphi_1,z_1,r_2,\varphi_2,z_2)\end{pmatrix}, \tag{22}$$

where $W_{ij}^{(ee)}(r_1,\varphi_1,z_1,r_2,\varphi_2,z_2)=\langle E_i(r_1,\varphi_1,z_1)E_j^*(r_2,\varphi_2,z_2)\rangle$, $(i,j=x,y,z)$, and

$$\begin{aligned} W_{xx}^{(ee)}(r_1,\varphi_1,z_1,r_2,\varphi_2,z_2)=&\frac{f^2n_1}{\lambda^2}\left\{\int_0^{\theta_{\max}}\int_0^{\theta_{\max}}\int_0^{2\pi}\int_0^{2\pi}\sqrt{\cos\theta_1\cos\theta_2}\sin\theta_1\sin\theta_2\right.\\ &\times\exp\{-ik_1[z_2\cos\theta_2+r_2\sin\theta_2\cos(\phi_2-\varphi_2)]\}\exp\{ik_1[z_1\cos\theta_1+r_1\sin\theta_1\cos(\phi_1-\varphi_1)]\}\\ &\times\{W_{xx}(\theta_1,\phi_1,\theta_2,\phi_2)[\cos\theta_1+\sin^2\phi_1(1-\cos\theta_1)][\cos\theta_2+\sin^2\phi_2(1-\cos\theta_2)]\\ &+W_{xy}(\theta_1,\phi_1,\theta_2,\phi_2)[\cos\theta_1+\sin^2\phi_1(1-\cos\theta_1)]\cos\phi_2\sin\phi_2(\cos\theta_2-1)\\ &+W_{yx}(\theta_1,\phi_1,\theta_2,\phi_2)\cos\phi_1\sin\phi_1(\cos\theta_1-1)[\cos\theta_2+\sin^2\phi_2(1-\cos\theta_2)]\\ &\left.+W_{yy}(\theta_1,\phi_1,\theta_2,\phi_2)\cos\phi_1\sin\phi_1(\cos\theta_1-1)\cos\phi_2\sin\phi_2(\cos\theta_2-1)\}d\theta_1\,d\theta_2\,d\phi_1\,d\phi_2\right\}, \end{aligned} \tag{23}$$

$$\begin{aligned} W_{xy}^{(ee)}(r_1,\varphi_1,z_1,r_2,\varphi_2,z_2)=&\frac{f^2n_1}{\lambda^2}\left(\int_0^{\theta_{\max}}\int_0^{\theta_{\max}}\int_0^{2\pi}\int_0^{2\pi}\sqrt{\cos\theta_1\cos\theta_2}\sin\theta_1\sin\theta_2\right.\\ &\times\exp\{-ik_1[z_2\cos\theta_2+r_2\sin\theta_2\cos(\phi_2-\varphi_2)]\}\exp\{ik_1[z_1\cos\theta_1+r_1\sin\theta_1\cos(\phi_1-\varphi_1)]\}\\ &\times\{W_{xx}(\theta_1,\phi_1,\theta_2,\phi_2)[\cos\theta_1+\sin^2\phi_1(1-\cos\theta_1)]\cos\phi_2\sin\phi_2(\cos\theta_2-1)\\ &+W_{xy}(\theta_1,\phi_1,\theta_2,\phi_2)[\cos\theta_1+\sin^2\phi_1(1-\cos\theta_1)][\cos\theta_2+\cos^2\phi_2(1-\cos\theta_2)]\\ &+W_{yx}(\theta_1,\phi_1,\theta_2,\phi_2)\cos\phi_1\sin\phi_1(\cos\theta_1-1)\cos\phi_2\sin\phi_2(\cos\theta_2-1)\\ &\left.+W_{yy}(\theta_1,\phi_1,\theta_2,\phi_2)\cos\phi_1\sin\phi_1(\cos\theta_1-1)[\cos\theta_2+\cos^2\phi_2(1-\cos\theta_2)]\}d\theta_1\,d\theta_2\,d\phi_1\,d\phi_2\right), \end{aligned} \tag{24}$$

$$\begin{aligned} W_{xz}^{(ee)}(r_1,\varphi_1,z_1,r_2,\varphi_2,z_2)=&-\frac{f^2n_1}{\lambda^2}\left(\int_0^{\theta_{\max}}\int_0^{\theta_{\max}}\int_0^{2\pi}\int_0^{2\pi}\sqrt{\cos\theta_1\cos\theta_2}\sin\theta_1\sin\theta_2\right.\\ &\times\exp\{-ik_1[z_2\cos\theta_2+r_2\sin\theta_2\cos(\phi_2-\varphi_2)]\}\exp\{ik_1[z_1\cos\theta_1+r_1\sin\theta_1\cos(\phi_1-\varphi_1)]\}\\ &\times\{W_{xx}(\theta_1,\phi_1,\theta_2,\phi_2)[\cos\theta_1+\sin^2\phi_1(1-\cos\theta_1)]\cos\phi_2\sin\theta_2\\ &+W_{xy}(\theta_1,\phi_1,\theta_2,\phi_2)[\cos\theta_1+\sin^2\phi_1(1-\cos\theta_1)]\sin\phi_2\sin\theta_2\\ &+W_{yx}(\theta_1,\phi_1,\theta_2,\phi_2)\cos\phi_1\sin\phi_1(\cos\theta_1-1)\cos\phi_2\sin\theta_2\\ &\left.+W_{yy}(\theta_1,\phi_1,\theta_2,\phi_2)\cos\phi_1\sin\phi_1(\cos\theta_1-1)\sin\phi_2\sin\theta_2\}d\theta_1\,d\theta_2\,d\phi_1\,d\phi_2\right), \end{aligned} \tag{25}$$

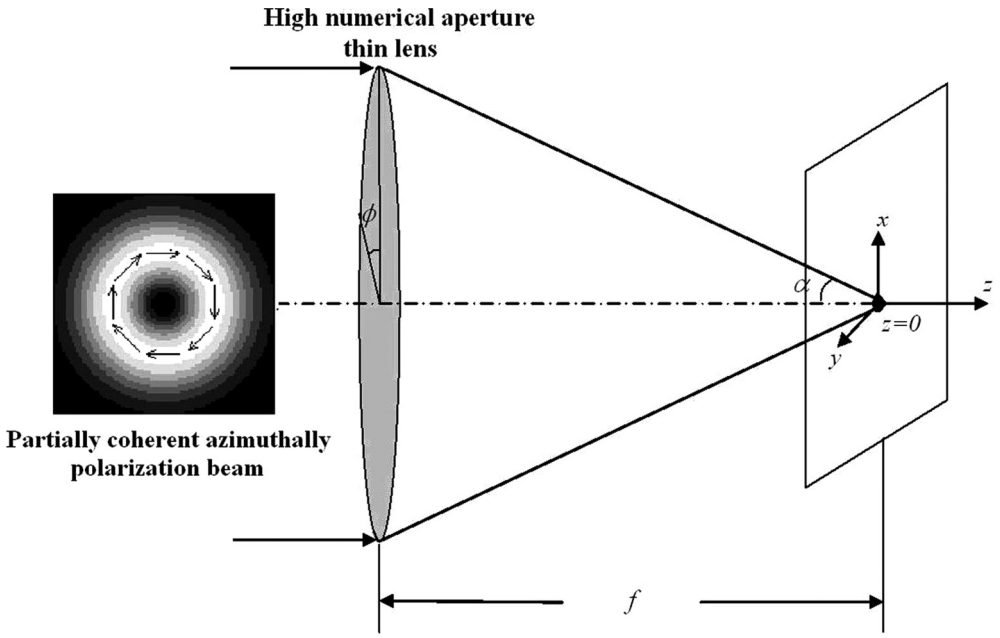

FIG. 7. Scheme of tight focusing system.

$$W_{yy}^{(ee)}(r_1,\varphi_1,z_1,r_2,\varphi_2,z_2) = \frac{f^2 n_1}{\lambda^2}\left(\int_0^{\theta_{\max}}\int_0^{\theta_{\max}}\int_0^{2\pi}\int_0^{2\pi}\sqrt{\cos\theta_1\cos\theta_2}\sin\theta_1\sin\theta_2\right.$$
$$\times\exp\{-ik_1[z_2\cos\theta_2 + r_2\sin\theta_2\cos(\phi_2-\varphi_2)]\}\exp\{ik_1[z_1\cos\theta_1 + r_1\sin\theta_1\cos(\phi_1-\varphi_1)]\}$$
$$\times\{W_{xx}(\theta_1,\phi_1,\theta_2,\phi_2)\cos\phi_1\sin\phi_1(\cos\theta_1-1)\cos\phi_2\sin\phi_2(\cos\theta_2-1)$$
$$+W_{xy}(\theta_1,\phi_1,\theta_2,\phi_2)\cos\phi_1\sin\phi_1(\cos\theta_1-1)[\cos\theta_2+\cos^2\phi_2(1-\cos\theta_2)]$$
$$+W_{yx}(\theta_1,\phi_1,\theta_2,\phi_2)[\cos\theta_1+\cos^2\phi_1(1-\cos\theta_1)]\cos\phi_2\sin\phi_2(\cos\theta_2-1)$$
$$\left.+W_{yy}(\theta_1,\phi_1,\theta_2,\phi_2)[\cos\theta_1+\cos^2\phi_1(1-\cos\theta_1)][\cos\theta_2+\cos^2\phi_2(1-\cos\theta_2)]\}d\theta_1\,d\theta_2\,d\phi_1\,d\phi_2\right), \tag{26}$$

$$W_{yz}^{(ee)}(r_1,\varphi_1,z_1,r_2,\varphi_2,z_2) = -\frac{f^2 n_1}{\lambda^2}\left(\int_0^{\theta_{\max}}\int_0^{\theta_{\max}}\int_0^{2\pi}\int_0^{2\pi}\sqrt{\cos\theta_1\cos\theta_2}\sin\theta_1\sin\theta_2\right.$$
$$\times\exp\{-ik_1[z_2\cos\theta_2 + r_2\sin\theta_2\cos(\phi_2-\varphi_2)]\}\exp\{ik_1[z_1\cos\theta_1 + r_1\sin\theta_1\cos(\phi_1-\varphi_1)]\}$$
$$\times\{W_{xx}(\theta_1,\phi_1,\theta_2,\phi_2)\cos\phi_1\sin\phi_1(\cos\theta_1-1)\cos\phi_2\sin\theta_2$$
$$+W_{xy}(\theta_1,\phi_1,\theta_2,\phi_2)\cos\phi_1\sin\phi_1(\cos\theta_1-1)\sin\phi_2\sin\theta_2$$
$$+W_{yx}(\theta_1,\phi_1,\theta_2,\phi_2)[\cos\theta_1+\cos^2\phi_1(1-\cos\theta_1)]\cos\phi_2\sin\theta_2$$
$$\left.+W_{yy}(\theta_1,\phi_1,\theta_2,\phi_2)[\cos\theta_1+\cos^2\phi_1(1-\cos\theta_1)]\sin\phi_2\sin\theta_2\}d\theta_1\,d\theta_2\,d\phi_1\,d\phi_2\right), \tag{27}$$

$$W_{zz}^{(ee)}(r_1,\varphi_1,z_1,r_2,\varphi_2,z_2) = \frac{f^2 n_1}{\lambda^2}\left\{\int_0^{\theta_{\max}}\int_0^{\theta_{\max}}\int_0^{2\pi}\int_0^{2\pi}\sqrt{\cos\theta_1\cos\theta_2}\sin\theta_1\sin\theta_2\right.$$
$$\times\exp\{-ik_1[z_2\cos\theta_2 + r_2\sin\theta_2\cos(\phi_2-\varphi_2)]\}\exp\{ik_1[z_1\cos\theta_1 + r_1\sin\theta_1\cos(\phi_1-\varphi_1)]\}$$
$$\times[W_{xx}(\theta_1,\phi_1,\theta_2,\phi_2)\cos\phi_1\sin\theta_1\cos\phi_2\sin\theta_2 + W_{xy}(\theta_1,\phi_1,\theta_2,\phi_2)\cos\phi_1\sin\theta_1\sin\phi_2\sin\theta_2$$
$$+W_{yx}(\theta_1,\phi_1,\theta_2,\phi_2)\sin\phi_1\sin\theta_1\cos\phi_2\sin\theta_2$$
$$\left.+W_{yy}(\theta_1,\phi_1,\theta_2,\phi_2)\sin\phi_1\sin\theta_1\sin\phi_2\sin\theta_2]d\theta_1\,d\theta_2\,d\phi_1\,d\phi_2\right\}, \tag{28}$$

$$W_{yx}^{(ee)}(r_1,\varphi_1,z_1,r_2,\varphi_2,z_2) = W_{xy}^{(ee)*}(r_2,\varphi_2,z_2,r_1,\varphi_1,z_1), \tag{29}$$

$$W_{zx}^{(ee)}(r_1,\varphi_1,z_1,r_2,\varphi_2,z_2) = W_{xz}^{(ee)*}(r_2,\varphi_2,z_2,r_1,\varphi_1,z_1), \tag{30}$$

$$W_{zy}^{(ee)}(r_1,\varphi_1,z_1,r_2,\varphi_2,z_2) = W_{yz}^{(ee)*}(r_2,\varphi_2,z_2,r_1,\varphi_1,z_1), \tag{31}$$

For a partially coherent AP beam, applying Eqs. (6)–(9), we can express $W_{xx}^{(ee)}(\theta_1,\phi_1,\theta_2,\phi_2)$, $W_{xy}^{(ee)}(\theta_1,\phi_1,\theta_2,\phi_2)$, $W_{yx}^{(ee)}(\theta_1,\phi_1,\theta_2,\phi_2)$, and $W_{yy}^{(ee)}(\theta_1,\phi_1,\theta_2,\phi_2)$ as follows:

$$W_{xx}^{(ee)}(\theta_1,\phi_1,\theta_2,\phi_2) = E_0^2\frac{f^2\sin\theta_1\sin\theta_2}{w_0^2} \times \exp\left[-f^2\frac{\sin^2\theta_1+\sin^2\theta_2}{w_0^2} - f^2\frac{\sin^2\theta_1+\sin^2\theta_2-2\sin\theta_1\sin\theta_2\cos(\phi_1-\phi_2)}{2\sigma_{xx}^2}\right]\sin\phi_1\sin\phi_2 \tag{32}$$

$$W_{xy}^{(ee)}(r_1,\phi_1,r_2,\phi_2) = -B_{xy}E_0^2\frac{f^2\sin\theta_1\sin\theta_2}{w_0^2} \times \exp\left[-f^2\frac{\sin^2\theta_1+\sin^2\theta_2}{w_0^2} - f^2\frac{\sin^2\theta_1+\sin^2\theta_2-2\sin\theta_1\sin\theta_2\cos(\phi_1-\phi_2)}{2\sigma_{xy}^2}\right]\sin\phi_1\cos\phi_2, \tag{33}$$

$$W_{yx}^{(ee)}(\theta_1,\phi_1,\theta_2,\phi_2) = W_{xy}^{(ee)*}(\theta_2,\phi_2,\theta_1,\phi_1), \tag{34}$$

$$W_{yy}^{(ee)}(\theta_1,\phi_1,\theta_2,\phi_2) = E_0^2\frac{f^2\sin\theta_1\sin\theta_2}{w_0^2} \times \exp\left[-f^2\frac{\sin^2\theta_1+\sin^2\theta_2}{w_0^2} - f^2\frac{\sin^2\theta_1+\sin^2\theta_2-2\sin\theta_1\sin\theta_2\cos(\phi_1-\phi_2)}{2\sigma_{yy}^2}\right]\cos\phi_1\cos\phi_2. \tag{35}$$

From Eq. (22), the total intensity distribution of the tightly focused partially coherent AP beam in the focal region is given by

$$\begin{aligned} I(r,\varphi,z) &= I_x(r,\varphi,z) + I_y(r,\varphi,z) + I_z(r,\varphi,z) \\ &= W_{xx}^{(ee)}(r,\varphi,z,r,\varphi,z) + W_{yy}^{(ee)}(r,\varphi,z,r,\varphi,z) \\ &\quad + W_{zz}^{(ee)}(r,\varphi,z,r,\varphi,z), \end{aligned} \tag{36}$$

Applying the derived formulas, we calculate in Fig. 8 the intensity distributions I_x, I_y, I_z, I, and the corresponding cross line ($y = 0$) of the total intensity distribution I of a tightly focused AP beam at the focal plane for different values of the correlation coefficients σ_{xx},σ_{yy},and σ_{xy} with $f = 1$ cm, $n_1 = 1.33$(water), $w_0 = 5$ mm, $\eta_{\text{power}} = 100$ mW, and $B_{xy} = 1$. As shown in Fig. 8, one sees that the intensity distribution I_z of a coherent or partially coherent tightly focused AP beam is equal to zero as expected, while I_x, I_y, and I of a tightly focused AP beam depend closely on the initial correlation coefficients (i.e., spatial coherence). For a completely coherent AP beam ($\sigma_{xx} = \sigma_{xy} = \sigma_{yy} =$ Infinity), I_x and I_y have two beamlets along the y and x directions, respectively, and I has a circular dark hollow beam profile. With the decrease of correlation coefficients, the two beamlet structures of the intensity distributions I_x and I_y gradually disappear, and the dark hollow beam profile of I also disappears gradually. For certain values of correlation coefficients ($\sigma_{xx} = \sigma_{xy} = \sigma_{yy} = 0.95w_0$), I_x and I_y have beam spots with "dumbbell" structure, and I has a circular flat-topped beam profile. For certain values of correlation coefficients ($\sigma_{xx} = \sigma_{xy} = \sigma_{yy} = 0.6w_0$), I_x and I_y have elliptical beam spots, and I has a Gaussian beam spot. When the correlation coefficients are very small ($\sigma_{xx} = \sigma_{xy} = \sigma_{yy} = 0.2w_0$), I_x, I_y, and I all have circular Gaussian beam spots.

Figure 9 shows the intensity distribution I of a tightly focused AP beam in the xz plane near focus for different values of the correlation coefficients. One finds from Fig. 9 that a dark channel is formed in the xz plane for a coherent tightly focused AP beam as expected. With the decrease of the correlation coefficients, the dark channel disappears gradually, and a bright beam spot in the xz plane is formed. The bright beam spot is of rectangular symmetry when the correlation coefficients are not very small, and the bright beam spot is of elliptical symmetry when the correlation coefficients are very small. Thus, decreasing the spatial coherence of an AP beam also provides a convenient way for shaping its tightly focused beam spot. Our results will be useful for material thermal processing, where a tightly focused flat-topped beam spot is required, [38] and for particle trapping, where a tightly focused dark hollow beam spot or bright beam spot is required as shown in Sec. V.

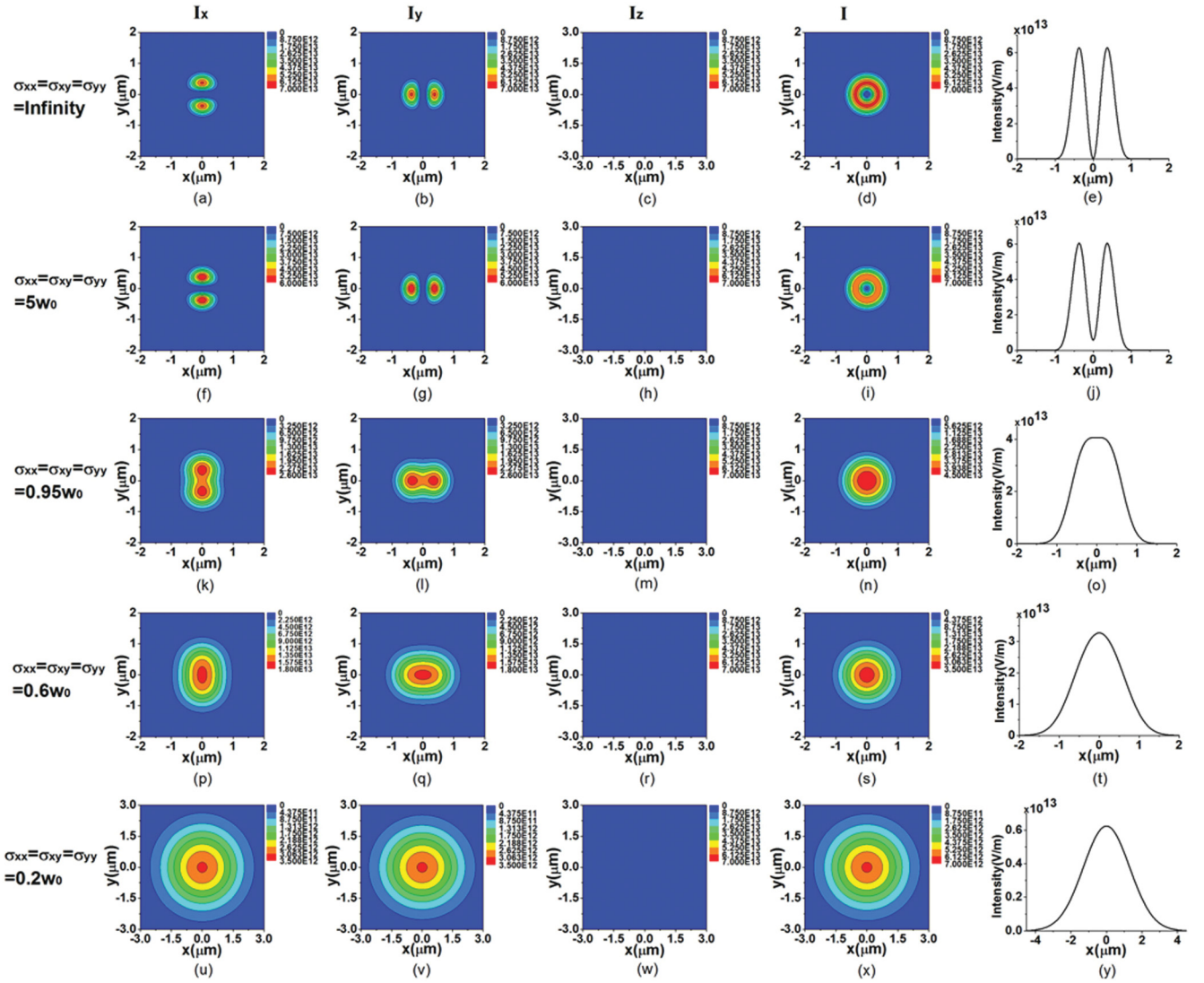

FIG. 8. (Color online) Intensity distributions I_x, I_y, I_z, I and the corresponding cross line ($y = 0$) of the total intensity distribution I of a tightly focused AP beam at the focal plane for different values of the correlation coefficients σ_{xx},σ_{yy},σ_{xy}.

V. RADIATION FORCES OF A TIGHTLY FOCUSED PARTIALLY COHERENT AP BEAM ON RAYLEIGH PARTICLES

In this section, we study the radiation forces of a tightly focused partially coherent AP beam on Rayleigh particles, and explore the effect of spatial coherence on the radiation forces.

When the radius a of a spherical particle is much smaller than the wavelength λ of the beam (generally $a < \lambda/20$), the Rayleigh scattering model is adopted to determine the radiation forces on the particle induced by the focused beam. [11,14,38–40] We assume a spherical Rayleigh particle with relative permittivity ε_2 and radius a is placed near the focus. According to the Rayleigh scattering theory, there are two kinds of radiation forces: gradient force $\vec{F}_{\text{grad}}$ and scattering force $\vec{F}_{\text{scat}}$, and they are expressed as [39]

$$\vec{F}_{\text{grad}}(r,\varphi,z) = \tfrac{1}{4}\text{Re}(\alpha)\vec{\nabla}|\vec{\mathbf{E}}(r,\varphi,z)|^2, \tag{37}$$

$$\vec{F}_{\text{scat}}(r,\varphi,z) = \frac{\sigma}{c}\langle\vec{S}(r,\varphi,z)\rangle + \sigma c\vec{\nabla}\langle\vec{L}_S(r,\varphi,z)\rangle, \tag{38}$$

where $\sigma = k\,\text{Im}(\alpha)/\varepsilon_0$ is defined as the total cross section of the particle, and α is the polarizability of the particle given by [39]

$$\alpha = \frac{\alpha_0}{1 - i\alpha_0 k^3/(6\pi\varepsilon_0)}, \tag{39}$$

with

$$\alpha_0 = 4\pi a^3\varepsilon_0\varepsilon_1(\varepsilon_2 - \varepsilon_1)/(\varepsilon_2 + 2\varepsilon_1). \tag{40}$$

Here ε_1 is the relative permittivity of the surrounding medium, $\langle\vec{S}(r,\varphi,z)\rangle$ is defined as the time-averaged Poynting vector of the light field, and $\langle\vec{L}_S(r,\varphi,z)\rangle$ is defined as the time-averaged spin density of the light field given by

$$\langle\vec{L}_S(r,\varphi,z)\rangle = \frac{\varepsilon_0}{4\omega i}[\vec{\mathbf{E}}(r,\varphi,z)\times\vec{\mathbf{E}}^*(r,\varphi,z)], \tag{41}$$

where ω is the frequency of the field. The first term of Eq. (38) is the traditional scattering force proportional to the Poynting vector of the light field, and the second term represents the scattering force proportional to the curl of the time-averaged spin density of the light field. [39]

For a tightly focused partially coherent beam, the term $|\vec{\mathbf{E}}(r,\varphi,z)|^2$ in Eq. (37) is expressed as

$$|\vec{\mathbf{E}}(r,\varphi,z)|^2 = I(r,\varphi,z) = W_{xx}^{(ee)}(r,\varphi,z,r,\varphi,z) + W_{yy}^{(ee)}(r,\varphi,z,r,\varphi,z) + W_{zz}^{(ee)}(r,\varphi,z,r,\varphi,z). \tag{42}$$

The time-averaged Poynting vector of the tightly focused partially coherent beam is given by [41,42]

$$\begin{aligned}\langle \vec{S}(r,\varphi,z)\rangle = \tfrac{1}{2} \lim_{\substack{r_1,r_2\to r\\ \varphi_1,\varphi_2\to\varphi\\ z_1,z_2\to z}} \mathrm{Re}\big\{&\big[W_{yz}^{(eh)}(r_1,\varphi_1,z_1,r_2,\varphi_2,z_2) - W_{zy}^{(eh)}(r_1,\varphi_1,z_1,r_2,\varphi_2,z_2)\big]\vec{e}_x\\ &+\big[W_{zx}^{(eh)}(r_1,\varphi_1,z_1,r_2,\varphi_2,z_2) - W_{xz}^{(eh)}(r_1,\varphi_1,z_1,r_2,\varphi_2,z_2)\big]\vec{e}_y\\ &+\big[W_{xy}^{(eh)}(r_1,\varphi_1,z_1,r_2,\varphi_2,z_2) - W_{yx}^{(eh)}(r_1,\varphi_1,z_1,r_2,\varphi_2,z_2)\big]\vec{e}_z\big\},\end{aligned} \tag{43}$$

where the terms $W_{ij}^{(eh)}(r_1,\varphi_1,z_1,r_2,\varphi_2,z_2) = \langle E_i(r_1,\varphi_1,z_1)H_j^*(r_2,\varphi_2,z_2)\rangle$ $(i,j = x,y,z)$ are the mixed cross-spectral densities for combining each scalar component of the electric field vector and the magnetic field vector. The term $H_j(r,\varphi,z)$ denotes the j component of the magnetic field vector of the tightly focused beam. According to Maxwell's equations, the term $W_{ij}^{(eh)}(r_1,\varphi_1,z_1,r_2,\varphi_2,z_2)$ can be expressed as [36,42]

$$W_{yz}^{(eh)}(r_1,\varphi_1,z_1,r_2,\varphi_2,z_2) = \frac{i}{\omega\mu_0}\left(\frac{\partial W_{yy}^{(ee)}(r_1,\varphi_1,z_1,r_2,\varphi_2,z_2)}{\partial x_2} - \frac{\partial W_{yx}^{(ee)}(r_1,\varphi_1,z_1,r_2,\varphi_2,z_2)}{\partial y_2}\right), \tag{44}$$

$$W_{zy}^{(eh)}(r_1,\varphi_1,z_1,r_2,\varphi_2,z_2) = \frac{i}{\omega\mu_0}\left(\frac{\partial W_{zx}^{(ee)}(r_1,\varphi_1,z_1,r_2,\varphi_2,z_2)}{\partial z_2} - \frac{\partial W_{zz}^{(ee)}(r_1,\varphi_1,z_1,r_2,\varphi_2,z_2)}{\partial x_2}\right), \tag{45}$$

$$W_{zx}^{(eh)}(r_1,\varphi_1,z_1,r_2,\varphi_2,z_2) = \frac{i}{\omega\mu_0}\left(\frac{\partial W_{zz}^{(ee)}(r_1,\varphi_1,z_1,r_2,\varphi_2,z_2)}{\partial y_2} - \frac{\partial W_{zy}^{(ee)}(r_1,\varphi_1,z_1,r_2,\varphi_2,z_2)}{\partial z_2}\right), \tag{46}$$

$$W_{xz}^{(eh)}(r_1,\varphi_1,z_1,r_2,\varphi_2,z_2) = \frac{i}{\omega\mu_0}\left(\frac{\partial W_{xy}^{(ee)}(r_1,\varphi_1,z_1,r_2,\varphi_2,z_2)}{\partial x_2} - \frac{\partial W_{xx}^{(ee)}(r_1,\varphi_1,z_1,r_2,\varphi_2,z_2)}{\partial y_2}\right), \tag{47}$$

$$W_{xy}^{(eh)}(r_1,\varphi_1,z_1,r_2,\varphi_2,z_2) = \frac{i}{\omega\mu_0}\left(\frac{\partial W_{xx}^{(ee)}(r_1,\varphi_1,z_1,r_2,\varphi_2,z_2)}{\partial z_2} - \frac{\partial W_{xz}^{(ee)}(r_1,\varphi_1,z_1,r_2,\varphi_2,z_2)}{\partial x_2}\right), \tag{48}$$

$$W_{yx}^{(eh)}(r_1,\varphi_1,z_1,r_2,\varphi_2,z_2) = \frac{i}{\omega\mu_0}\left(\frac{\partial W_{yz}^{(ee)}(r_1,\varphi_1,z_1,r_2,\varphi_2,z_2)}{\partial y_2} - \frac{\partial W_{yy}^{(ee)}(r_1,\varphi_1,z_1,r_2,\varphi_2,z_2)}{\partial z_2}\right). \tag{49}$$

The term $\langle \vec{L}_S(r,\varphi,z)\rangle$ of a tightly focused partially coherent beam is expressed as

$$\begin{aligned}\langle \vec{L}_S(r,\varphi,z)\rangle &= \frac{\varepsilon_0}{4\omega i}\langle \vec{\mathbf{E}}(r,\varphi,z)\times\vec{\mathbf{E}}^*(r,\varphi,z)\rangle = \frac{\varepsilon_0}{4\omega i}[\vec{e}_x(\langle E_yE_z^*\rangle - \langle E_zE_y^*\rangle) + \vec{e}_y(\langle E_zE_x^*\rangle - \langle E_xE_z^*\rangle) + \vec{e}_z(\langle E_xE_y^*\rangle - \langle E_yE_x^*\rangle)]\\ &= \frac{\varepsilon_0}{4\omega i}\big\{\vec{e}_x\big(W_{yz}^{(ee)}(r,\varphi,z,r,\varphi,z) - W_{zy}^{(ee)}(r,\varphi,z,r,\varphi,z)\big) + \vec{e}_y\big(W_{zx}^{(ee)}(r,\varphi,z,r,\varphi,z) - W_{xz}^{(ee)}(r,\varphi,z,r,\varphi,z)\big)\\ &\quad +\vec{e}_z\big(W_{xy}^{(ee)}(r,\varphi,z,r,\varphi,z) - W_{yx}^{(ee)}(r,\varphi,z,r,\varphi,z)\big)\big\}\\ &= \frac{\varepsilon_0}{2\omega}\mathrm{Im}\big[W_{yz}^{(ee)}(r,\varphi,z,r,\varphi,z)\vec{e}_x - W_{xz}^{(ee)}(r,\varphi,z,r,\varphi,z)\vec{e}_y + W_{xy}^{(ee)}(r,\varphi,z,r,\varphi,z)\vec{e}_z\big],\end{aligned} \tag{50}$$

and the term $\vec{\nabla}\times\langle \vec{L}_S(r,\varphi,z)\rangle$ can be expressed as

$$\begin{aligned}\vec{\nabla}\times\langle \vec{L}_S(r,\varphi,z)\rangle = \frac{\varepsilon_0}{2\omega}\mathrm{Im}\Bigg[&\left(\frac{\partial W_{xy}^{(ee)}(r,\varphi,z,r,\varphi,z)}{\partial y} + \frac{\partial W_{xz}^{(ee)}(r,\varphi,z,r,\varphi,z)}{\partial z}\right)\vec{e}_x\\ &+\left(\frac{\partial W_{yz}^{(ee)}(r,\varphi,z,r,\varphi,z)}{\partial z} - \frac{\partial W_{xy}^{(ee)}(r,\varphi,z,r,\varphi,z)}{\partial x}\right)\vec{e}_y - \left(\frac{\partial W_{xz}^{(ee)}(r,\varphi,z,r,\varphi,z)}{\partial x} + \frac{\partial W_{yz}^{(ee)}(r,\varphi,z,r,\varphi,z)}{\partial y}\right)\vec{e}_z\Bigg].\end{aligned} \tag{51}$$

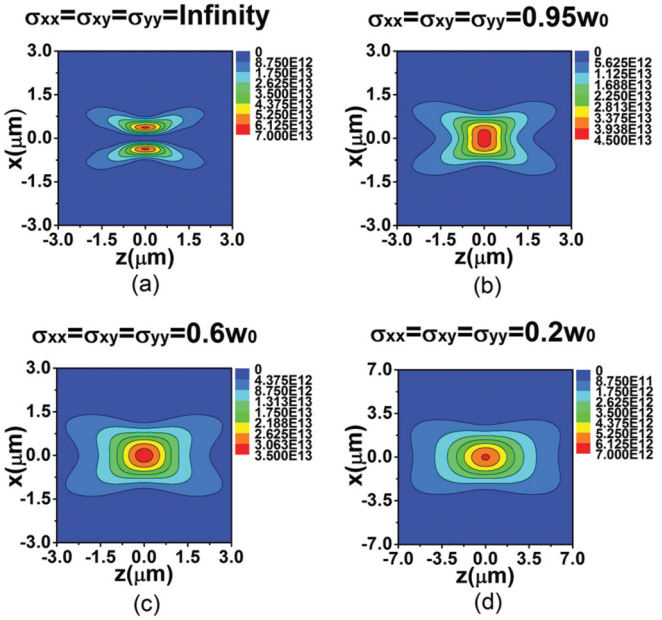

FIG. 9. (Color online) Intensity distribution I of a tightly focused AP beam in the xz plane near focus for different values of the correlation coefficients $\sigma_{xx},\sigma_{yy},\sigma_{xy}$.

Applying Eqs. (22)–(51), we can study the effect of spatial coherence on the radiation forces of a tightly focused partially coherent AP beam on Rayleigh particles. In the following text, we set $a = 30$ nm, $n_1 = 1.33$(water), $\lambda = 1.047$ μm, $f = 1$ cm, $w_0 = 5$ mm, $\eta_{\text{power}} = 100$ mW, and $B_{xy} = 1$.

To trap a particle stably, the gradient force should be larger than the sum of scattering forces, i.e., $R = \vec{F}_{\text{grad}}(r,\varphi,z)/\vec{F}_{\text{scat}}(r,\varphi,z) > 1$. Furthermore, the particle usually suffers the Brownian motion due to the thermal fluctuation from the surrounding medium (water in our case), thus the gradient force also should be larger than the Brownian force. Following the fluctuation-dissipation theorem of Einstein, the magnitude of the Brownian force is expressed as $|F_B| = (12\pi\kappa a k_B T)^{1/2}$ [43] with κbeing the viscosity of the surrounding medium, k_B being the Boltzmann constant, and T being the temperature of the surrounding medium. In our case, for water, $\kappa = 7.977 \times 10^{-4}$Pa at $T = 300$ K, [44] and the magnitude of the Brownian force is equal to 1.93×10^{-3} pN.

We calculate in Fig. 10 the radiation forces of a tightly focused AP beam on a Rayleigh particle with $\varepsilon_2 = 1$ (air bubble) for different values of the correlation coefficients σ_{xx},σ_{xy}, and σ_{yy}. For the convenience of comparison, the Brownian force is also shown in Fig. 10. The sign of the radiation forces determines the direction of the force: for positive $F_{\text{scat},x}$ or $F_{\text{scat},z}$, the direction of the scattering force is along the $+x$ or $+z$ direction; for positive $F_{\text{grad},x}$ and $F_{\text{grad},z}$, the direction of the gradient force is along the $+x$ or $+z$ direction. When the correlation coefficients are large (i.e., spatial coherence is high), we find from Figs. 10(a1) and 10(b2) that the transverse gradient force is much larger than the Brownian force and the transverse scattering force, and there exists one transverse stable equilibrium point at

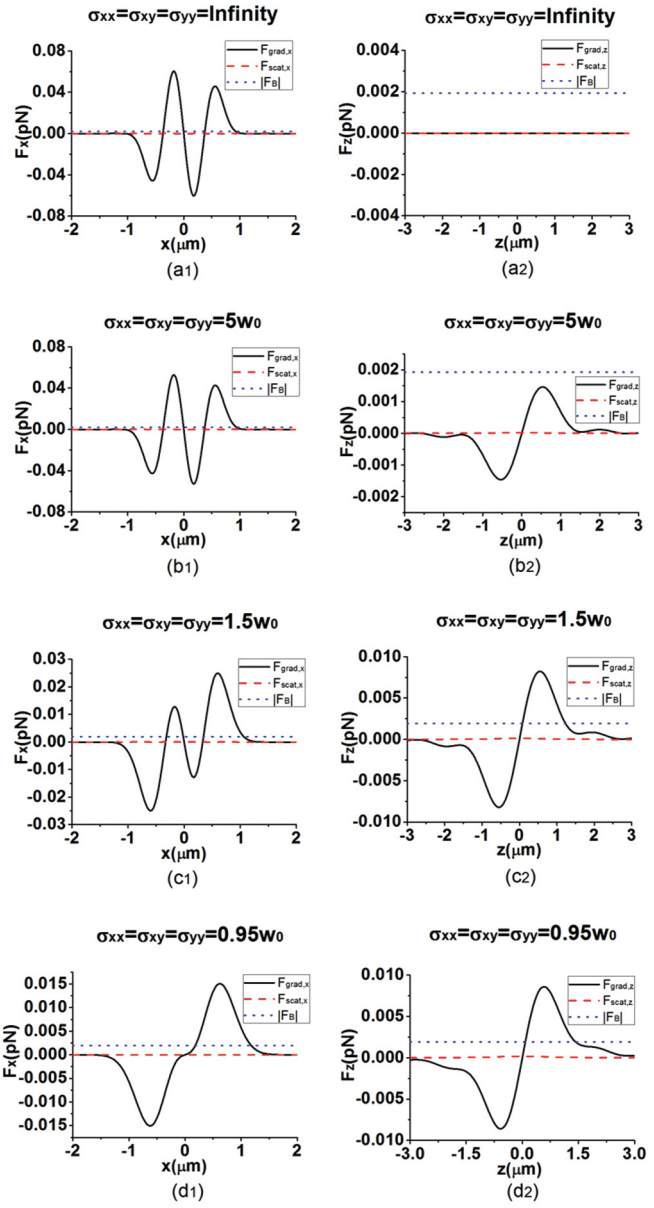

FIG. 10. (Color online) Radiation forces of a tightly focused AP beam on a Rayleigh particle with $\varepsilon_2 = 1$ (air bubble) for different values of the correlation coefficients $\sigma_{xx},\sigma_{xy},\sigma_{yy}$.

the focal plane, while the longitudinal gradient force and the longitudinal scattering force are much smaller than the Brownian force [see Figs. 10(a2) and 10(b2)]. Thus, a tightly focused AP beam with high spatial coherence can be used to trap transversely a Rayleigh particle whose refractive index is smaller than that of the ambient near the focus. If one wants to trap the air bubble in a three-dimensional space, three focused AP beams (orthogonal to each other) with high spatial coherence are required to form a closed dark region, which can be used to trap the air bubble stably. With the decrease of the correlation coefficients, the magnitude of the gradient force $F_{\text{grad},x}$ decreases, while the magnitude of the gradient force $F_{\text{grad},z}$ increases. For intermediate values of the correlation

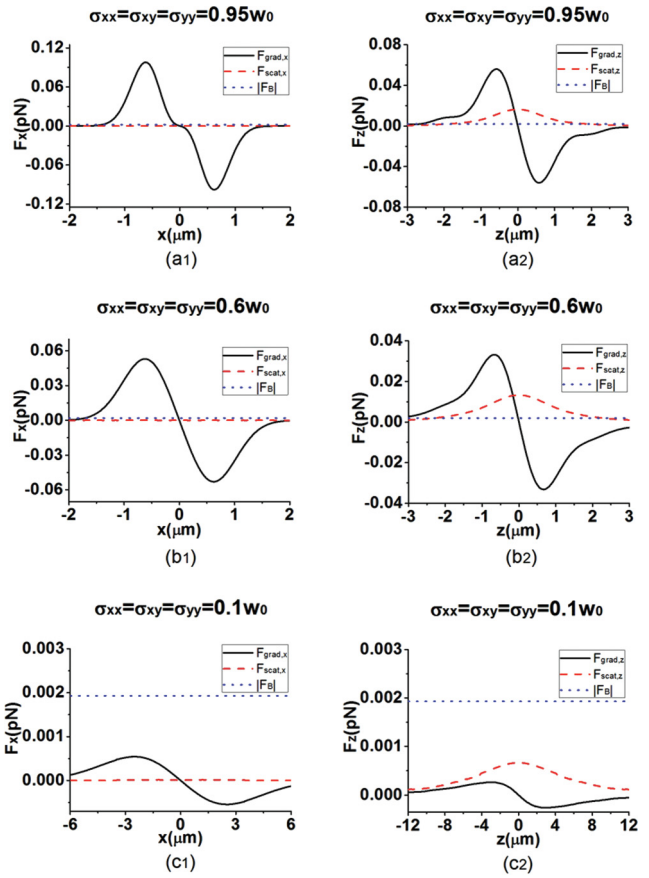

FIG. 11. (Color online) Radiation forces of a tightly focused AP beam on a Rayleigh particle with $\varepsilon_2 = -54 + 5.9i$ (gold particle) for different values of the correlation coefficients $\sigma_{xx}, \sigma_{xy}, \sigma_{yy}$

coefficients, there still exists one transverse stable equilibrium point at the focal plane [see Fig. 10(c1)] and the gradient force $F_{\text{grad},z}$ near the focus is much larger than the Brownian force, which means that a tightly focused AP beam with intermediate spatial coherence can be used to trap the air bubble transversely, and accelerate the air bubble along the z direction near the focus. When the correlation coefficients are small, one finds from Fig. 10(d1) and 10(d2) that there is no stable equilibrium point at the focal plane, while the air bubble still can be accelerated along the z direction near the focus.

We calculate in Fig. 11 the radiation forces of a tightly focused AP beam on a Rayleigh particle with $\varepsilon_2 = -54 + 5.9i$ (gold particle) for different values of the correlation coefficients σ_{xx}, σ_{xy}, and σ_{yy}. For the case of $\sigma_{xx} = \sigma_{xy} = \sigma_{yy} = 0.95w_0$, we see that the gradient forces $F_{\text{grad},x}$ and $F_{\text{grad},z}$ are larger than the Brownian force, $F_{\text{grad},z}$ is larger than $F_{\text{scat},z}$, and there exists one stable equilibrium point at the focus [see Figs. 11(a1) and 11(a2)]. Thus a tightly focused AP beam with suitable spatial coherence can be used to trap a Rayleigh particle whose refractive index is larger than that of the ambient. With the decrease of the correlation coefficients, the magnitudes of the gradient forces and the scattering force decreases [see Figs. 11(b1), 11(b2), 11(c1), and 11(c2)]. For the case of $\sigma_{xx} = \sigma_{xy} = \sigma_{yy} = 0.1w_0$, the gradient forces and the scattering force all become smaller than the Brownian force, thus a tightly focused AP beam with extremely low spatial coherence cannot be used to trap a Rayleigh particle.

VI. CONCLUSION

In summary, we have outlined briefly the theoretical model for a partially coherent AP beam and its paraxial propagation formula based on the unified theory of coherence and polarization. We have carried out experimental generation of an AP beam with variable spatial coherence and measured its propagation properties, and our experimental results verified the theoretical predictions. The effects of spatial coherence on the intensity distribution of an AP beam focused by a high NA objective lens have been illustrated numerically, and it was found that the beam spot of a tightly focused AP beam can be shaped by varying the spatial coherence, i.e., focused dark hollow, flat-topped, and Gaussian beam spots can be obtained by choosing suitable spatial coherence. Through studying the radiation forces on Rayleigh particles induced by a tightly focused AP beam, we have found that a tightly focused AP beam can be used to trap a Rayleigh particle whose refractive index is larger or smaller than that of the ambient by varying its initial spatial coherence. Our results will be useful for particle trapping and material thermal processing.

ACKNOWLEDGMENTS

This work is supported by the National Natural Science Foundation of China under Grants No. 10904102, No. 61008009, and No. 11104195; the Foundation for the Author of National Excellent Doctoral Dissertation of PR China under Grant No. 200928; the Natural Science Foundation of Jiangsu Province under Grant No. BK2009114; the Huo Ying Dong Education Foundation of China under Grant No. 121009; the Key Project of Chinese Ministry of Education under Grant No. 210081; the Universities Natural Science Research Project of Jiangsu Province Grants No. 10KJB140011 and No. 11KJB140007; a Project Funded by the Priority Academic Program Development of Jiangsu Higher Education Institutions; and the Innovation Plan for Graduate Students in the Universities of Jiangsu Province under Grant No. CXLX11_0064.

[1] Q. Zhan, Adv. Opt. Photon. **1**, 1 (2009).
[2] B. Sick, B. Hecht, and L. Novotny, Phys. Rev. Lett. **85**, 4482 (2000).
[3] L. Novotny, M. R. Beversluis, K. S. Youngworth, and T. G. Brown, Phys. Rev. Lett. **86**, 5251 (2001).
[4] R. Dorn, S. Quabis, and G. Leuchs, Phys. Rev. Lett. **91**, 233901 (2003).
[5] A. Ciattoni, B. Crosignani, P. DiPorto, and A. Yariv, Phys. Rev. Lett. **94**, 073902 (2005).
[6] Y. I. Salamin, Phys. Rev. A **82**, 013823 (2010).

[7] S. Yan and B. Yao, Phys. Rev. A **77**, 023827 (2008).
[8] H. Wang, L. Shi, B. Lukyanchuk, C. J. R. Sheppard, and C. T. Chong, Nat. Photonics **2**, 501 (2008).
[9] W. Chen, D. Abeysinghe, R. Nelson, and Q. Zhan, Nano Lett. **9**, 4320 (2009).
[10] Y. Cai, Q. Lin, H. T. Eyyuboglu, and Y. Baykal, Opt. Express **16**, 7665 (2008).
[11] Q. Zhan, Opt. Express **12**, 3377(2004).
[12] S. Yan and B. Yao, Phys. Rev. A **76**, 053836 (2007).
[13] F. Peng, B. Yao, S. Yan, W. Zhao, and M. Lei, J. Opt. Soc. Am. B **26**, 2242 (2009).
[14] Y. Zhang, B. Ding, and T. Suyama, Phys. Rev. A **81**, 023831 (2010).
[15] N. Lindlein, S. Quabis, U. Peschel, and G. Leuchs, Opt. Express **15**, 5827 (2007).
[16] A. A. Tovar, J. Opt. Soc. Am. A **15**, 2705 (1998).
[17] R. Oron, S. Blit, N. Davidson, and A. A. Friesem, Appl. Phys. Lett. **77**, 3322 (2000).
[18] Z. Bomzon, V. Kleiner, and E. Hasman, Appl. Phys. Lett. **79**, 1587 (2001).
[19] M. Fridman, G. Machavariani, N. Davidson, and A. A. Friesem, Appl. Phys. Lett. **93**, 191104 (2008).
[20] J. Li, K. I. Ueda, M. Musha, A. Shirakawa, and L. X. Zhong, Opt. Lett. **31**, 2969 (2006).
[21] M. Fridman, G. Machavariani, N. Davidson, and A. A. Friesem, Appl. Phys. Lett. **93**, 191104 (2008).
[22] K. S. Youngworth and T. G. Brown, Opt. Express **7**, 77 (2000).
[23] S. Quabis, R. Dorn, M. Eberler, O. Glokl, and G. Leuchs, Opt. Commun. **179**, 1 (2000).
[24] D. P. Biss and T. G. Brown, Opt. Express **9**, 490 (2001).
[25] Q. Zhan and J. R. Leger, Opt. Express **10**, 324 (2002).
[26] E. Y. S. Yew and C. J. R. Sheppard, Opt. Lett. **32**, 3417 (2007).
[27] X. Hao, C. Kuang, T. Wang, and X. Liu, Opt. Lett. **35**, 3928 (2010).
[28] B. Tian and J. Pu, Opt. Lett. **36**, 2014 (2011).
[29] P. Wrobel, J. Pniewski, T. J. Antosiewicz, and T. Szoplik, Phys. Rev. Lett. **102**, 183902 (2009).
[30] W. Chen, R. L. Nelson, and Q. Zhan, Opt. Lett. **37**, 581(2012).
[31] X. Jiao, S. Liu, Q. Wang, X. Gan, P. Li, and J. Zhao, Opt. Lett. **37**, 1041 (2012).
[32] Y. Dong, Y. Cai, C. Zhao, and M. Yao, Opt. Express **19**, 5979 (2011).
[33] F. Wang, Y. Cai, Y. Dong, and O. Korotkova, Appl. Phys. Lett. **100**, 051108 (2012).
[34] E. Wolf, Phys. Lett. A **312**, 263 (2003).
[35] E. Wolf, *Introduction to the Theory of Coherence and Polarization of Light* (Cambridge University Press, Cambridge, 2007).
[36] L. Mandel and E. Wolf, *Optical Coherence and Quantum Optics* (Cambridge University Press, Cambridge, 1995).
[37] F. Wang and Y. Cai, J. Opt. Soc. Am. A **24**, 1937 (2007).
[38] D. W. Coutts, IEEE J. Quantum Electron. **38**, 1217 (2002).
[39] S. Albaladejo, M. I. Marqués, M. Laroche, and J. J. Sáenz, Phys. Rev. Lett. **102**, 113602 (2009).
[40] Y. Harada and T. Asakura, Opt. Commun. **124**, 529 (1996).
[41] J. Li, B. Lu, and S. Zhu, Opt. Express **17**, 11399 (2009).
[42] L. Zhang, F. Wang, Y. Cai, and O. Korotkova, Opt. Commun. **284**, 1111 (2011).
[43] K. Okamoto and S. Kawata, Phys. Rev. Lett. **83**, 4534 (1999).
[44] J. Kestin, M. Sokolov, and W. A. Wakeham, J. Phys. Chem. Ref. Data **7**, 941 (1978).